International Journal of Numerical Methods for Heat & Fluid Flow

1983

A numerical study of double flow focusing micro-jets

Rizwan Zahoor
Department of Fluid Dynamics and Thermodynamics, Faculty of Mechanical Engineering, University of Ljubljana, Ljubljana, Slovenia

Saša Bajt
Center for Free-Electron Laser Science CFEL, Deutsches Elektronen-Synchrotron DESY, Hamburg, Germany and The Hamburg Centre for Ultrafast Imaging, Universität Hamburg, Hamburg, Germany, and

Božidar Šarler
Department of Fluid Dynamics and Thermodynamics, Faculty of Mechanical Engineering, University of Ljubljana, Ljubljana, Slovenia, Slovenia and Laboratory for Simulation of Materials and Processes, Institute of Metals and Technology, Ljubljana, Slovenia

Received 1 July 2024
Revised 4 September 2024
Accepted 5 September 2024

Abstract

Purpose – Double flow-focusing nozzles (DFFNs) form a coaxial flow of primary liquid with micro-crystalline samples, surrounded by secondary liquid and focusing gas. This paper aims to develop an experimentally validated numerical model and assess the performance of micro-jets from a DFFN as a function of various operating parameters for the water–ethanol–helium system, revealing the jet's stability, diameter, length and velocity.

Design/methodology/approach – The physical model is formulated in the mixture-continuum formulation, which includes coupled mass, momentum and species transport equations. The model is numerically formulated within the finite volume method–volume of fluid approach and implemented in OpenFOAM to allow for a non-linear variation of the fluid's material properties as a function of the mixture concentration. The numerical results are compared with the experimental data.

Findings – A sensitivity study of jets with Reynolds numbers between 12 and 60, Weber numbers between 4 and 120 and capillary numbers between 0.2 and 2.0 was performed. It was observed that jet diameters and lengths get larger with increased primary and secondary fluid flow rates. Increasing gas flow rates produces thinner, shorter and faster jets. Previously considered pre-mixed and linear mixing models substantially differ from the accurate representation of the water–ethanol mixing dynamics in DFFNs. The authors demonstrated that Jouyban–Acree mixing model fits the experimental data much better.

The funding for this research is provided by the Center for Free-Electron Laser Science (CFEL) under the project: Innovative Methods for Imaging with the use of X-ray Free-Electron Laser (XFEL) and Synchrotron Sources: simulation of gas-focused micro-jets, and Slovenian Grant and Innovation Agency (ARIS) within Program Group P2-0162 and Project J2-4477. This work is also partly supported by the Cluster of Excellence "CUI: Advanced Imaging of Matter" of the Deutsche Forschungsgemeinschaft (DFG)-EXC 2056-project ID390715994.

International Journal of Numerical Methods for Heat & Fluid Flow
Vol. 35 No. 6, 2025
pp. 1983-2003
Emerald Publishing Limited
0961-5539
DOI 10.1108/HFF-07-2024-0480

Originality/value – The mixing of primary and secondary liquids in the jet produced by DFFN is numerically modelled for the first time. This study provides novel insights into mixing dynamics in such micro-jets, which can be used to improve the design of DFFNs.

Keywords Serial femtosecond crystallography, Sample delivery, Double flow focusing, Water–ethanol mixing, Jet properties, Finite volume method, Volume of fluid

Paper type Research paper

1. Introduction

Microfluidics covers the complex world of fluid dynamics at the microscopic scales and has applications ranging from material chemistry (Günther and Jensen, 2006), drug screening/delivery (Fontana *et al.*, 2016; Sun *et al.*, 2019) and bioengineering (Finehout and Tian, 2009) to food safety (Nilghaz *et al.*, 2021). Microfluidic devices can be used to create small bubbles (Garstecki *et al.*, 2004), droplets (Baroud *et al.*, 2010), jets (Gañán-Calvo *et al.*, 2010) and sheets (Koralek *et al.*, 2018). In this paper, we are particularly interested in microfluidic devices which deliver samples into intense x-ray beams produced by large x-ray facilities such as synchrotrons and x-ray free electron lasers (XFELs). The development of these intense x-ray sources opened up many new scientific areas. One of them, which is based on the idea of how to overcome radiation damage in imaging macromolecules (Neutze *et al.*, 2000), is serial femtosecond crystallography (SFX) (Chapman *et al.*, 2011). It revolutionised the field of protein crystallography and is widely used at XFEL facilities (Barends *et al.*, 2022). Micron-sized protein crystals, considered previously unusable, can now be exploited to obtain diffraction patterns from which one can determine a protein structure or follow triggered chemical processes. This is because in SFX experiments, diffraction patterns of small protein crystals are acquired before they are destroyed by intense, femtosecond x-ray pulses (Barty *et al.*, 2012). Protein crystals can be brought into the x-ray beam in different ways. The most commonly used way is via liquid micro-jets. It has the advantage of keeping protein crystals in a hydrated environment, while they are exposed to XFEL pulses. The sample delivery systems and their effectiveness in various experimental settings have been extensively reviewed (Barends *et al.*, 2022; Martiel *et al.*, 2019), and it is clear that the quality of SFX experiments is intricately linked to the stability and efficiency of the micro-jet delivery system. Jet-focusing techniques have improved thanks to many experimental and numerical studies over the past decade (Schlichting, 2015). Nevertheless, many challenges remain to keep up with the technological improvements of x-ray sources and detectors.

Worldwide, only five operating XFEL facilities deliver femtosecond pulses in hard x-ray regime. One of them is European XFEL (Altarelli, 2011), which started operating in 2017 and is located in Schenefeld, Germany. This XFEL delivers x-ray pulses in bursts or "trains" with a train repetition rate of 10 Hz. Each train is only a few microseconds long but can contain up to 2,700 x-ray pulses. This corresponds to 4.5 MHz maximum pulse repetition rate. Although such a high repetition rate allows faster data collection, it also poses major challenges for optics, detectors and sample delivery.

Here, we are primarily interested in sample delivery. Liquid jets used in experiments at European XFEL have to be fast enough to bring the sample in and out of the interaction region before the arrival of the next x-ray pulse, which requires speeds of at least 50 m/s (Wiedorn *et al.*, 2018). Such velocities can be achieved by accelerating the liquid with a high-pressure gas (Gañán-Calvo, 1998). The gas dynamic virtual nozzles (GDVNs) (DePonte *et al.*, 2008; Weierstall *et al.*, 2012) are based on this concept. These and other microdevices are now routinely manufactured using modern additive three-dimensional

printing technology. For example, two-photon stereolithography is one of the three-dimensional printing methods that offers submicron precision. This enables fast and easy prototyping of small nozzles (Knoška *et al.*, 2020; Nelson *et al.*, 2016). In addition to high speeds, these jets also need to be thin to reduce the background coming from the liquid and to minimise sample consumption. Ideally, the jets are at least 50 µm long to avoid illuminating and damaging nozzles with the intense x-rays. Millisecond-long pulse trains with a repetition rate of 10 Hz leave many precious samples unexposed to x-rays. This is especially true when jets are created by GDVNs, which require approximately 10–40 µl/min flow rates to produce stable jets (Botha and Fromme, 2023).

Double flow-focusing nozzles (DFFNs) (Oberthuer *et al.*, 2017) represent a pivotal advancement over the conventional alternatives such as Rayleigh jets (Rayleigh, 1879), plate-orifice nozzle (Gañán-Calvo, 1998) and GDVNs (DePonte *et al.*, 2008). DFFNs initially reported by Gañán-Calvo *et al.* (2007) integrated an additional immiscible secondary fluid between the primary sample-carrying liquid and the outer focusing gas (conventional plate-orifice nozzles). The improved DFFN design (Oberthuer *et al.*, 2017) includes an additional converging secondary liquid capillary inside a standard converging GDVN. This results in thinner, longer and more stable jets while reducing sample consumption (GDVN: 40 µl/min versus DFFN: 2 µl/min). An additional advantage is that jet-forming conditions only need to be fulfilled by the outer focusing liquid (Vega *et al.*, 2010). This allows variations in the sample carrying core liquid flow rates and liquids without interruption in the jetting, which is convenient when changing the sample (innermost capillary) during the experiment. Because of the excellent characteristics of ethanol for forming fine, stable jets and for reducing icing when the jets are used in a vacuum, it is commonly used as a secondary sheath liquid between the focusing gas and primary sample-carrying buffer (Oberthuer *et al.*, 2017).

The multiphase jet flows within the channels of the DFFN involve sophisticated interactions of diverse cohesive and disruptive forces. These forces strongly correlate with the material properties of the working fluids, ultimately dictating the behaviour of resulting jets emanating from DFFNs. The rheological properties of the involved fluids can help quantify the actively involved forces, such as the shear generated at the interfaces, which is directly associated with the fluid viscosity (Zahoor *et al.*, 2024). Experimental studies, limited to the investigations of overall jetting performance in terms of their stability, length and diameters, can profit from numerical simulations to better understand forces acting upon these jets and their interplay.

Indeed, numerical simulations have significantly advanced the basic understanding of jets (Herrada *et al.*, 2008; Kovačič *et al.*, 2024; Zahoor *et al.*, 2018c). They have been successfully used in the geometric optimisation of plate-orifice (Vega *et al.*, 2010), converging GDVNs (Zahoor *et al.*, 2018a) and converging-diverging nozzles for jet focusing (Šarler *et al.*, 2021). Additionally, numerical simulations have added value in investigating various jetting liquids (Zahoor *et al.*, 2020) and focusing gases (Zahoor *et al.*, 2018b). Recent simulations have yielded reasonable agreement with experimentally obtained results regarding jetting, dripping and whipping (Kovačič *et al.*, 2024). The fluid dynamics aspects of nozzles are elaborated in a contemporary monograph (Montanero, 2024).

Despite the significant strides in numerical simulations, exploring DFFN jet flows has been limited. Previous studies have either assumed non-mixing conditions between primary and secondary fluids (Oberthuer *et al.*, 2017) or adopted pre-mixed primary and secondary fluids at both inlets (Belšak *et al.*, 2021). Against this backdrop, the primary objective of this paper is to build a robust model for DFFNs, capable of accommodating dynamics of

diffusion and convection mixing involved between the primary and the secondary fluids along the jet.

2. Numerical model

The cylindrical symmetry of DFFN allows an axisymmetric numerical approach. Similar previous approaches have successfully revealed the underlying physical phenomena of jet focusing in GDVN nozzles (Herrada *et al.*, 2008; Zahoor *et al.*, 2021). The whipping jet instabilities and the secondary breakups, which can, in principle, be simulated (Kovačič *et al.*, 2024), are not of interest here, as such jets are unsuitable for SFX experiments.

In our numerical model, we assume an incompressible, Newtonian, laminar, two-phase flow involving gas and liquid phase, with the liquid phase composed of water and ethanol binary system. A schematic of the DFFN nozzle geometry under consideration is shown in Figure 1.

The considered problem is based on the following mass, momentum and concentration equations:

$$\nabla \cdot \mathbf{v} = 0, \tag{1}$$

$$\partial(\rho \mathbf{v})/\partial t + \nabla \cdot (\rho \mathbf{v}\mathbf{v}) = -\nabla p + \nabla \cdot \left[\mu\left(\nabla \mathbf{v} + \nabla \mathbf{v}^{\mathrm{T}}\right)\right] + \mathbf{f}_{\sigma}, \tag{2}$$

$$\partial C/\partial t + \nabla \cdot (\mathbf{v}C) = \nabla \cdot (D \nabla C), \tag{3}$$

with $\mathbf{v}$ denoting velocity, t time, p pressure, ρ density, μ viscosity and $\mathbf{f}_{\sigma}$ body force, originating from the surface tension. The gravity was neglected in these simulations. C stands for the ethanol concentration (molar fraction), bounded between $C = 0$ (pure water) and $C = 1$ (pure ethanol). The diffusion coefficient of ethanol into water is defined by D. The moving interphase boundary between the liquid and the gas phases is treated using the

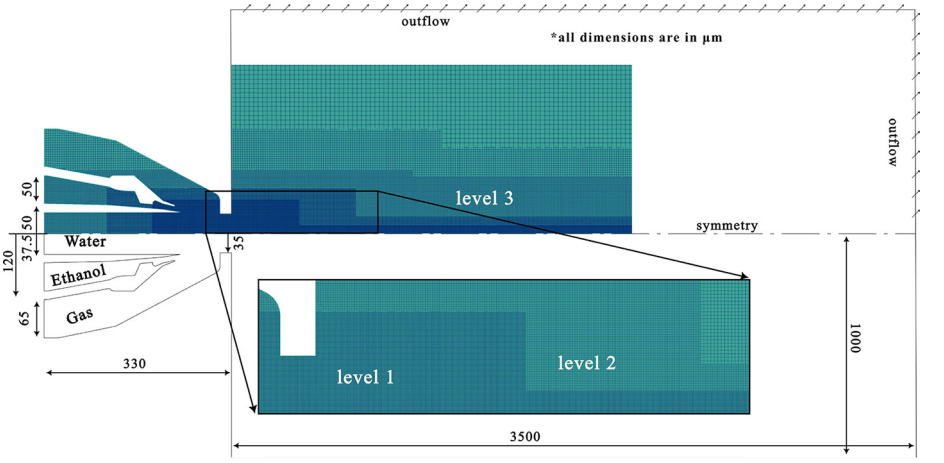

Source: Figure by authors

Figure 1. Scheme of the geometry and discretisation of double flow-focusing nozzles (cell sizes of level 1 = 0.5 µm, level 2 = 1.0 µm and level 3 = 2.0 µm)

volume of fluid (VOF) method. A phase function α, bounded between 0 (gas) and 1 (liquid), is advected in the domain using an interface advection equation:

$$\partial\alpha/\partial t + \mathbf{v}\cdot\nabla\alpha = 0. \tag{4}$$

For the surface tension forces, the continuum surface force (Brackbill *et al.*, 1992) model is used ($\mathbf{f}_\sigma = \sigma\kappa\nabla\alpha$) with σ representing the surface tension. The interface curvature κ is calculated from the interface normal $\hat{\mathbf{n}}$ as $\kappa(\alpha) = -\nabla\cdot\hat{\mathbf{n}} = \nabla\alpha/|\nabla\alpha|$. The material properties and flow field in the mixture-continuum formulation are calculated as:

$$\begin{aligned} \theta &= \theta_l\alpha + \theta_g(1-\alpha) \\ \mathbf{v} &= \left[\mathbf{v}_l\alpha + \mathbf{v}_g(1-\alpha)\right]/\rho \end{aligned} \tag{5}$$

where θ_l can either denote density ρ_l, viscosity μ_l or surface tension σ. The density ρ_l, viscosity μ_l and surface tension σ of the assumed two-component water–ethanol liquid phase are calculated using Jouyban–Acree model (Jouyban and Acree, 1998) at T = 293 K:

$$\theta_l = exp\left[C_w ln\,(\theta_w) + C ln\,(\theta_e) - \mathrm{A}_\theta CC_w/T - \mathrm{B}_\theta CC_w(C_w - \mathrm{C})/T + \mathrm{C}_\theta CC_w(C_w - \mathrm{C})^2/T\right], \tag{6}$$

with the concentration of water C_w related to the concentration of ethanol as $C_w = 1 - C$. θ_w and θ_e stand for the related pure water and ethanol properties, respectively. The parameters involved in equation (6) are given in Table 1 (Khattab *et al.*, 2012) for density $\theta \equiv \rho$, viscosity $\theta \equiv \mu$ and surface tension $\theta \equiv \sigma$.

The finite volume method (FVM) (Ferziger and Perić, 2002; Moukalled *et al.*, 2016; Versteeg and Malalasekera, 2007) is used to solve the related two-phase (gas–liquid) and three-species (gas–water–ethanol) problem. The gas–liquid interface is solved by the algebraic VOF model (Hirt and Nichols, 1981). The interface compression approach addresses the inherent interface smearing of VOF (Weller, 2008).

Open source FVM-VOF code OpenFOAM (Greenshields, 2022) is used, which tackles the axisymmetric problems by a three-dimensional 5° wedge domain (Figure 1), with the bottom aligned to the symmetry line. The DFFN computational domain is discretised into approximately 200,000 hexa-dominant finite volumes, arranged so that the maximum refinements (minimum cell size of 0.5 µm) are ensured in the vicinity of jet formation. The cell sizes gradually increase away from the liquid jet, reaching a maximum of 16 µm.

The choices of control volume and outlet domain dimensions (with a length 3,500 µm and radius 1,000 µm) are determined from a previously conducted mesh independence and

Table 1. Fitting coefficients in equation (6) for density, viscosity and surface tension model

Material property	A_θ	B_θ	C_θ
Density	30.808	18.274	13.890
Viscosity	724.652	729.357	976.050
Surface tension	488.012	640.785	1073.310

Source: Table by authors

domain size study (Zahoor *et al.*, 2018c). Eight distinct boundary patches are selected for imposing boundary conditions, as detailed in Table 2, where Q_p and Q_s represent flow rate of primary liquid (water: Q_w) and secondary liquid (ethanol: Q_e), respectively.

The solution relies on at least second-order schemes. Gaussian finite-volume integration (LeVeque, 2002) is used for calculating derivative terms, and a second-order vanLeer total variation diminishing scheme (van Leer, 1979) is applied for convective terms. A total variation diminishing limited linear V scheme is used to interpolate variables from cell to face. The transient terms are -addressed using a blended second-order Crank–Nicolson scheme, allowing setting up a blending weight coefficient ϕ. The value of the blending coefficient decides if the scheme operates in a pure Euler ($\phi = 0$) or implicit ($\phi = 1$) regime. The present solution setup uses $\phi = 0.9$ to balance accuracy and robustness.

The PIMPLE algorithm is used for pressure–velocity coupling. A Courant number (Courant *et al.*, 1967) condition is enforced (≤ 0.25) to adopt the time step. A comprehensive documentation of the implementation and guidelines for using the described numerical schemes can be found in Moukalled *et al.* (2016).

The operating fluids include water as the primary fluid, ethanol as a secondary fluid and helium as a focusing gas. The material properties of pure operating fluids are summarised in Table 3. OpenFOAM solver "interFoam" was extended by solving an additional concentration equation (3) in the liquid phase. The mixture library in "interFoam" was upgraded to include the Jouyban–Acree [equation (6)] model. This represents a most accurate mixing model representing the physicochemical properties of binary mixtures (Jouyban and Acree, 2021). It accurately predicts the solubility data and enables the modelling of mixture properties as a function of solubility data and temperature (Khattab

Table 2. Boundary conditions at computational boundary patches

Patch	Velocity	Pressure	Phase fraction	Concentration
Inlet water	$Q_p = Q_w$	$\partial p/\partial n = 0$	$\alpha = 1$	$C = 0$
Inlet ethanol	$Q_s = Q_e$	$\partial p/\partial n = 0$	$\alpha = 1$	$C = 1$
Inlet gas	$\dot{m}_g$	$\partial p/\partial n = 0$	$\alpha = 0$	$C = 0$
Walls	$\mathbf{v} = 0$	fixedFluxPressure[a]	$\partial\alpha/\partial n = 0$	$\partial C/\partial n = 0$
Outlet	$\partial\mathbf{v}/\partial n = 0$	$p = 1 \times 10^5$ Pa	$\partial\alpha/\partial n = 0$	$\partial C/\partial n = 0$
Front	Wedge[b]			
Back	Wedge			

Notes: [a]The pressure gradient is set such that the flux on the boundary is specified by the velocity boundary condition; [b]A special boundary condition to enforce cyclic conditions between the two patches
Source: Table by authors

Table 3. Reference material properties of operating fluids at temperature and pressure conditions (T = 293 K and 101,325 pa)

Fluid	Density [kgm^{-3}]	Viscosity [Pas]	Surface tension [Nm^{-1}]
Water	998	1.0×10^{-03}	0.0724
Ethanol	791	1.14×10^{-03}	0.0224
Helium	0.164	1.96×10^{-05}	–

Source: Table by authors

et al., 2012). These material properties of the water–ethanol–helium system are used in the model equations (1)–(3).

The numerical simulations are initialised such that the primary and secondary capillaries are filled with water and ethanol, respectively, while the rest of the domain is filled with stagnant helium. The simulations are calculated up to 0.001 s on 64 Intel (R) Xeon (R) processors.

3. Results and discussion

A hydrodynamic based liquid jet focusing from DFFN nozzle is investigated. It involves primary (water) and secondary (ethanol) fluids, supplied through respective capillaries and focused with outer focusing helium gas. In contrast to a similar study (Gañán-Calvo *et al.*, 2007), it uses miscible primary and secondary liquids that tend to mix as they flow out of the feeding capillaries and are focused by a gas to form a jet. Such a convective and diffusive mixing process results in spatial variation of material properties, thus influencing the fluid dynamics of the jet.

As water and ethanol show a non-linear mixing (Khattab *et al.*, 2012), it is essential to model the local variation in material properties accurately. The used Jouyban–Acree model for water–ethanol mixture material properties at 293 K is shown in Figure 2.

It is seen in Figure 2 that with the increase of ethanol concentration, the density almost linearly drops from pure water density to ethanol density. The mixture viscosity, on the other hand, is peaked at $C \approx 0.25$. With the increase of ethanol concentration, viscosity increases to approximately 2.4 mPas and then steadily drops towards the viscosity of pure ethanol. The surface tension rapidly decreases from 0.072 Nm^{-1} up to C ≈ 0.2, experiencing a plateau up to C ≈ 0.6, followed by a less steep decrease towards pure ethanol value.

For such a non-linear behaviour of mixture material properties, oversimplification of either non-mixing, linear mixing or supply of pre-mixed water–ethanol solution from both primary and secondary capillaries in the previous numerical studies (Belšak *et al.*, 2021; Oberthuer *et al.*, 2017) provide only qualitative estimates. Such assumptions ignore local spatial variations of the material properties at micro scales. For example, Figure 3 shows a comparison of the pre-mixed water–ethanol solution (50% by mass) at both liquid inlets with

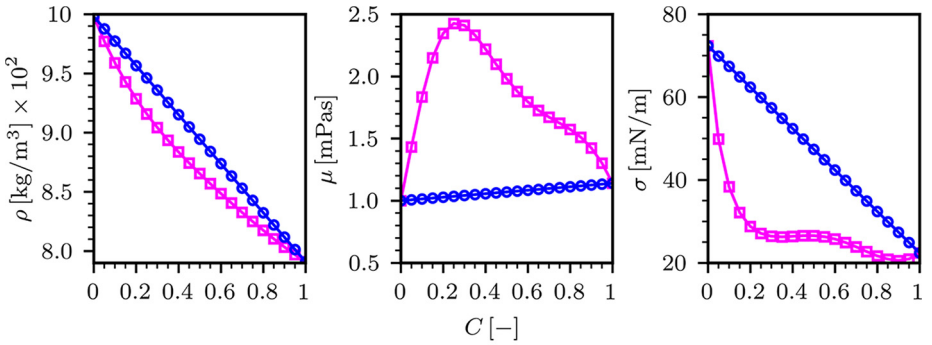

Notes: $C = 0$ represents pure water; $C = 1$ pure ethanol
Source: Figure by authors

Figure 2. Density, viscosity and surface tension of water–ethanol mixture as a function of ethanol concentration in mixture with linear (○) and Jouyban–Acree (□) mixing models at 293 K

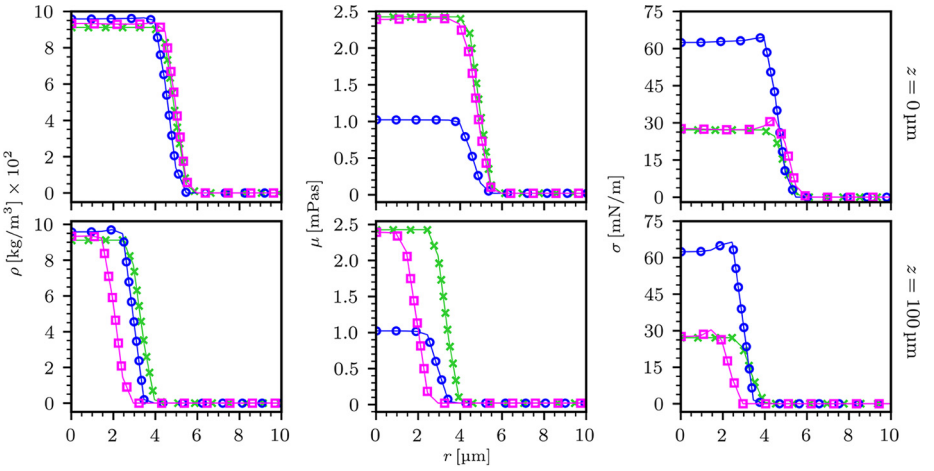

Source: Figure by authors

Figure 3. Radial density, viscosity and surface tension profiles of the water–ethanol mixture at nozzle outlet (top) and at 100 µm from nozzle outlet (bottom) with pre-mixed (×), linear (○) and Jouyban–Acree (□) mixing models at 293 K

Jouyban–Acree and linear mixing. The material properties of the pre-mixed binary solution are spatially invariant compared to linear and Jouyban–Acree mixture models. Additionally, the pre-mixed case works with the assumption that the water and ethanol are fully mixed at both liquid inlets. Such assumption of constant or linear viscosity changes limits the accurate determination of shear forces at the liquid gas interfaces by over/under-estimating them.

Additionally, already mixed binary solutions at liquid inlets do not represent the actual working of DFFN flows, where water and ethanol are separately supplied and show non-linear spatial mixing. It is also essential to include a proper surface tension force (Zahoor *et al.*, 2020), which alters the jet characteristics (Figure 4) if not correctly accounted for. The surface tension force acts as a momentum sink, scaled approximately $2\sigma/D_j$ (Gañán-Calvo, 1998), showing that it has the same important role as the jet diameter on the jet length. The DFFNs manipulate the surface tension force because of secondary fluid focus and mixing, which is not the case with conventional GDVNs. The implemented non-linear Jouyban–Acree model for water–ethanol mixing is the most accurate (Khattab *et al.*, 2012) describing the relevant material properties of the mixture.

After implementing the Jouyban–Acree mixing model, we carried out a mesh independence study. Three different cell sizes were used, and the resulting jet characteristics were analysed in terms of jet diameter and length, as shown in Figure 5.

As jet characteristics do not differ much between the cell size of 0.5 µm and 0.25 µm, further numerical simulations were carried out with a cell size of 0.5 µm. The experimental validation of the numerical model was performed on mesh-independent results. This experimental data was collected at CFEL (DESY, Hamburg). The DFFN manufacturing/printing, experimental setup and data collection procedures were extensively discussed (Knoška *et al.*, 2020; Oberthuer *et al.*, 2017). Figure 6 compares a snapshot of the jet with a numerically simulated one. In Figure 7, the average experimental jet diameters and jet velocities, measured in three positions downstream, are shown together with the minimum

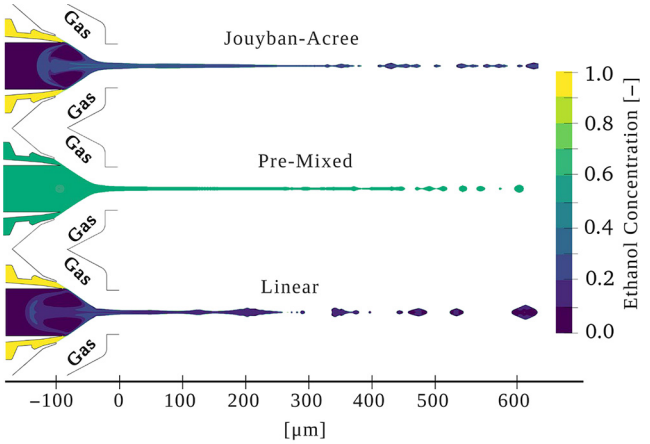

Source: Figure by authors

Figure 4. Instantaneous representation of a liquid jet with Jouyban–Acree, pre-mixed and linear mixing models

and maximum observed values. They are compared with the numerically simulated temporal diameter and velocity data. The experimental jet velocities were obtained using dual pulse imaging laser-induced fluorescence (Knoška *et al.*, 2020). Overall, a good match between experimental and numerical results is observed.

The reason behind comparing experimentally averaged data with the temporal numerical results is a difference in time resolution between the experiments and numerical simulations. The imaging instrumentation has a lower frame rate than the simulations (1 µs in the present case). The average values of both numerical and experimental data are similar over a larger time interval.

Two limiting cases of DFFN operation were considered first:

(1) injection of pure water from both primary and secondary capillaries; and

(2) pure water replacement in a secondary capillary with pure ethanol.

The comparison in Figure 8 shows how the water–ethanol mixing influences material properties and the resulting jets. It reveals that the water–ethanol mixture helps to counter the destabilising forces and provides a longer and more stable jet than the pure water case.

We performed a parametric study to understand the influence of water, ethanol and helium flow rates. In our first study, the primary liquid (water) flow rate varied from 2 µl/min to 20 µl/min, while ethanol and gas flow rates remained constant at 10 µl/min and 5 mg/min, respectively. In the second study, the water and gas flow rates were kept constant at 10 µl/min and 5 mg/min, while the ethanol flow rate varied from 2 µl/min to 20 µl/min. In the third study, we kept water and ethanol flow rates constant at 10 µl/min and varied the gas flow rate from 2 mg/min to 20 mg/min. Once the simulation passed the initial transient, the jet diameters, lengths and velocities were averaged over 100 µs time interval, as shown in Figure 9.

The nozzles used in SFX experiments and resulting jets and droplets are of sizes in the micrometre range, so it is reasonable to question whether slip flow conditions might occur on

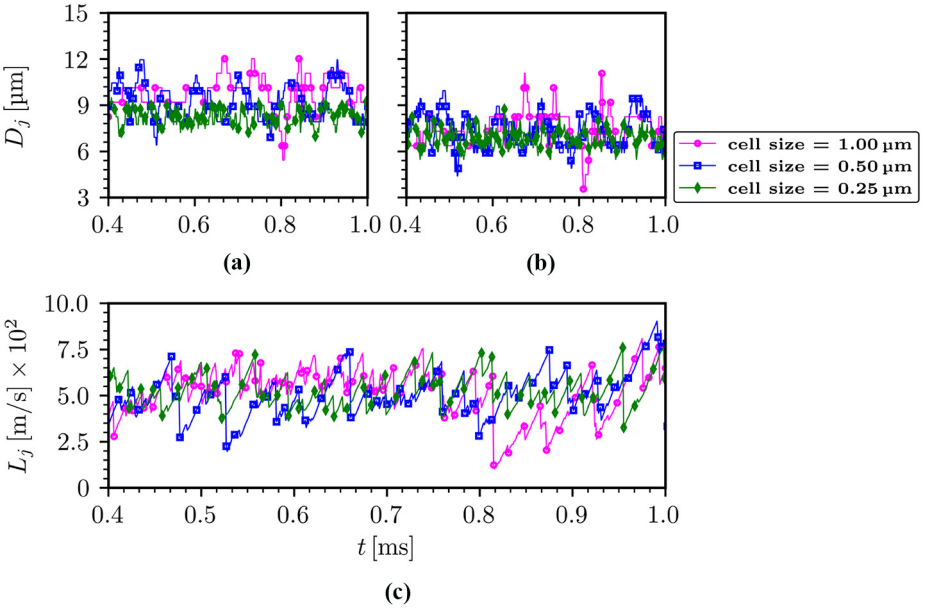

Notes: The jet dimeters at (a) nozzle outlet; (b) 100 µm downstream in the outlet chamber; (c) jet lengths are presented for water Q_w = 10 µl/min, ethanol Q_e = 10 µl/min and helium flow rates m_g = 5 mg/min
Source: Figure by authors

Figure 5. Mesh independence study of double flow focusing nozzle jets for three different cell sizes of 1.0 µm, 0.50 µm and 0.25 µm

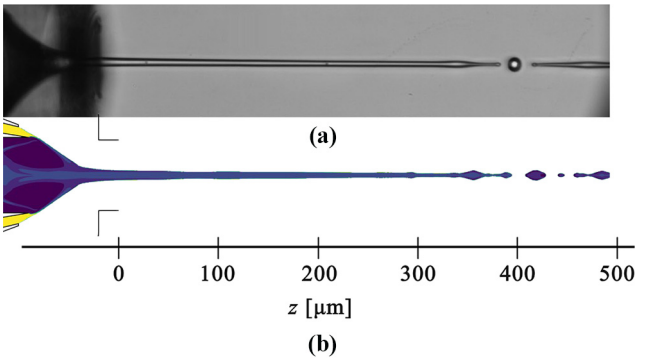

Source: Figure by authors

Figure 6. Snapshot of (a) experimentally and (b) numerically obtained jets with Q_w = 10 µl/min, Q_e = 10 µl/min and m_g = 5 mg/min

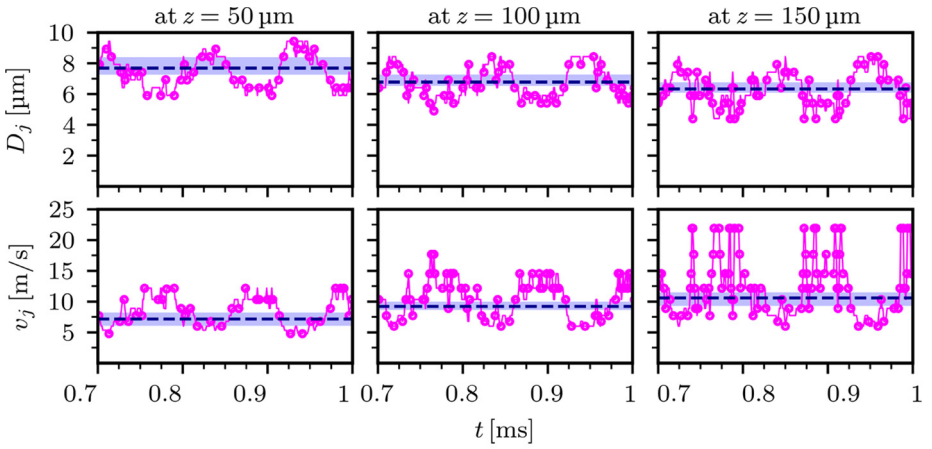

Notes: The dashed line represents the average value, while the shaded region denotes the minimum and maximum value occurring over 100 experimental data records
Source: Figure by authors

Figure 7. Evolution of numerical (○) jet diameters and velocities at 50 µm, 100 µm and 150 µm compared with experimentally obtained average (---) jet diameters and jet velocities measured with dual pulse imaging laser-induced fluorescence for Q_w = 10 µl/min, Q_e = 10 µl/min and m_g = 5 mg/min

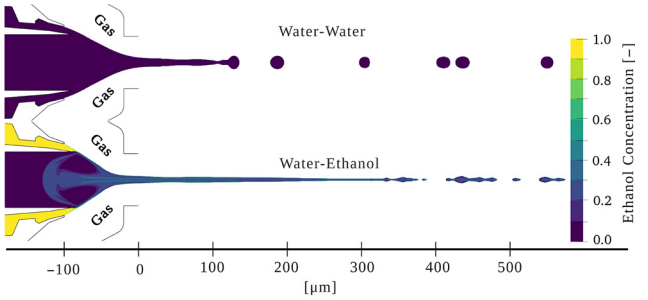

Note: The gas flow rate is m_g = 5 mg/min
Source: Figure by authors

Figure 8. Comparison of double flow focusing nozzle operation with water (Q_w = 10 µl/min) from primary and secondary capillaries (top) and water from primary and ethanol from secondary capillary (bottom) at Q_w = 10 µl/min and Q_e = 10 µl/min, respectively

surfaces. We have considered this possibility and evaluated whether the flow regime remains within the full no-slip condition.

To assess the applicability of the no-slip condition, we examined the Knudsen number $Kn = \lambda/L$, defined as the ratio of the molecular mean free path $\lambda = k_B/\sqrt{2}\pi d^2 \rho R_{\text{gas}}$ to a characteristic length scale L. With the characteristics length of our system being nozzle opening (L = 30 µm) and helium molecular diameter d = 260 p.m., ρ = 0.164 kgm^{-3} and

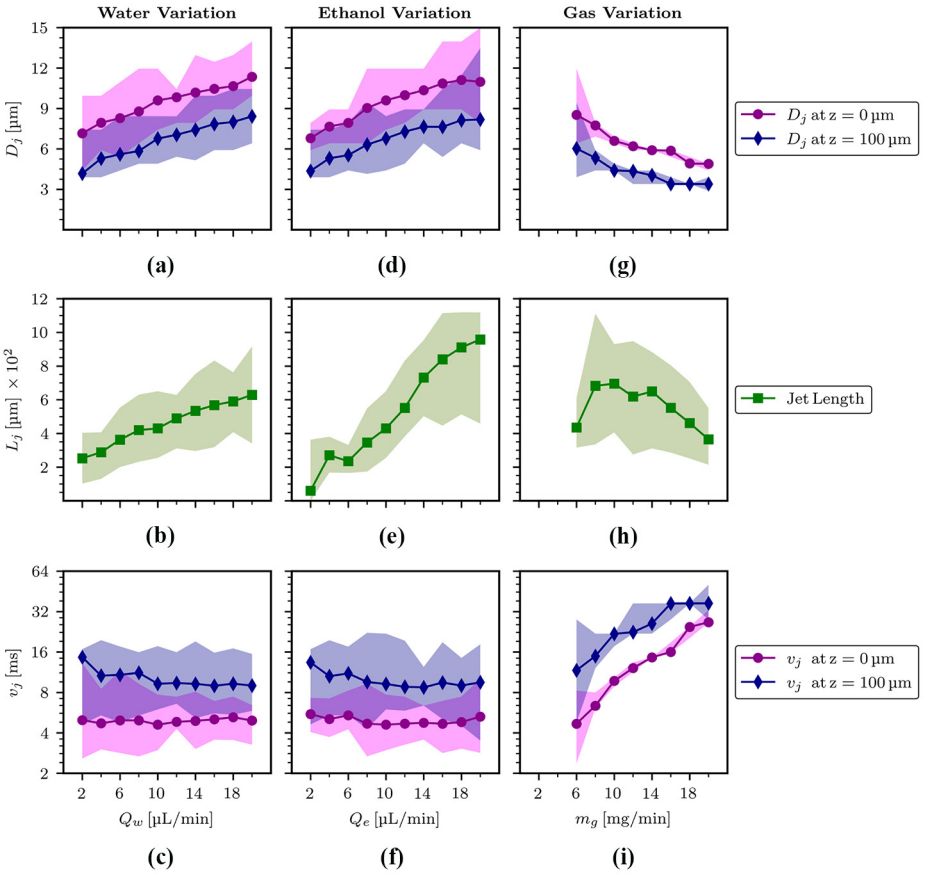

Notes: Average jet diameter (d), length (e) and velocity (f) as a function of ethanol flow rate at water flow rate of 10 µl/min and gas flow rate of 5 mg/min. Average jet diameter (g), length (h) and velocity (i) as a function of gas flow rate at a water flow rate of 10 µl/min and ethanol flow rate of 10 µl/min. The shaded regions represent the interval between the minimum and the maximum values
Source: Figure by authors

Figure 9. Average jet diameter (a), length (b) and velocity (c) as a function of water flow rate at ethanol flow rate of 10 µl/min and gas flow rate of 5 mg/min

Boltzmann constant k_B = 1.380649 × 10^{-23} J/K, the Knudsen number was calculated to be 0.0044. This value is less than 0.01, indicating that the flow remains within the continuum regime.

With 20 mg/min of the highest analysed inlet gas flow rate, the gas velocity of 850 ms^{-1} is reached at nozzle's opening with R_{throat} = 35 µm. Under these conditions, a 3 µm diameter jet with 35 ms^{-1} velocity is achieved. The maximum liquid Reynolds number (Re = $\rho v_l R_j/\mu_l$) = 100, calculated with liquid density 1,000 kgm^{-3} and viscosity 0.001 Pas, while the gas Reynolds number (Re = $\rho v_g R_{throat}/\mu_g$) = 250 at the nozzle opening with gas density 0.164

kgm^{-3} and viscosity 1.98e-05 Pas. These Reynolds numbers are significantly smaller than the threshold values of turbulent flows. Thus, a laminar flow assumption is justified.

Figures 9(a), (d) and (g), show that the numerically calculated jet diameters decrease in the downstream direction. The decrease does not align with the assumption (Herrada *et al.*, 2008) that the jet diameter remains the same downstream of the outlet chamber. With the increase in water flow rate from 2 µl/min to 20 µl/min, the jet diameters and lengths increase, but their velocities decrease [Figures 9(a), (b) and (c),]. A similar trend is observed when the water flow rate (10 µl/min) and gas flow rate (5 mg/min) are constant, while the ethanol flow rate is increased from 2 µl/min to 20 µl/min (Figures 9(d), (e) and (f)]. The jets become thinner, faster and longer than when we varied the water flow rate. When the gas flow rate was increased from 2 mg/min to 20 mg/min, the gas flow rate had to be increased up to 5 mg/min before the jet stabilized, as the focusing momentum was otherwise too low to overcome the inertial and surface tension forces. Increasing the gas flow to 6 mg/min resulted in a thick, short and slow jet. A further increase produced more extended jets. In combination with higher gas flow rates, the jets became thinner, shorter and faster [Figures 9(g), (h) and (i),]. The momentum sinks related to surface tension force in thinner jets became stronger, explaining shorter jets at higher gas flow rates.

Another interesting observation is the extent of mixing between water and ethanol, as seen in Figure 10, and the resulting variations in material properties. There is no jetting if using only pure ethanol and no water (0 µl/min) from the central capillary. However, even though the water flow rate is zero, the boundary and initial conditions assume that the

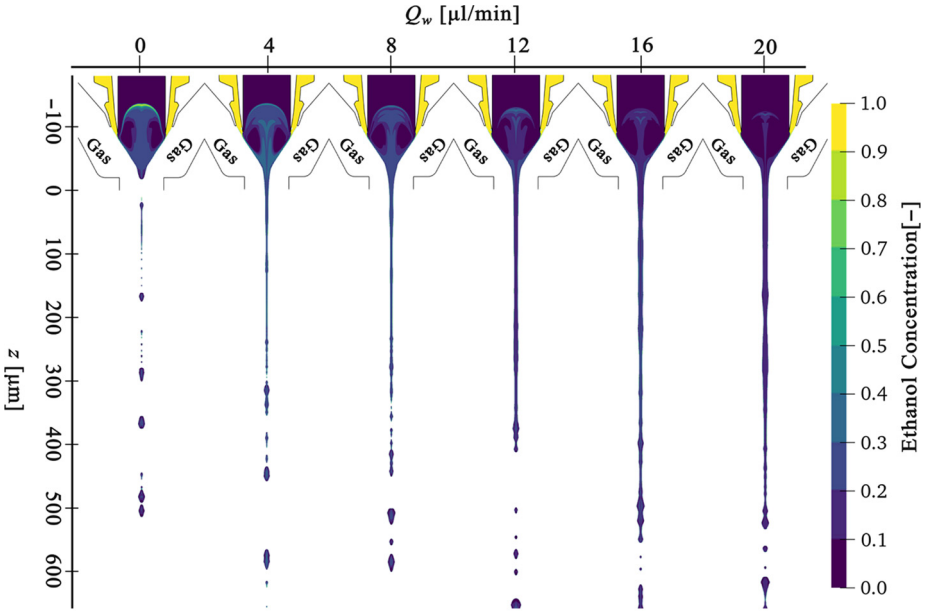

Source: Figure by authors

Figure 10. Comparison of micro-jet shape and ethanol concentration as a function of water flow rate at constant ethanol and gas flow rates of 10 µl/min and 5 mg/min, respectively

primary capillary is filled with water and that the ethanol, which flows from the secondary capillary, mixes with the water. As expected, an increase in water flow rate results in a decrease in relative ethanol concentration. At 20 µl/min of water flow rate, the jet liquid consists primarily of water. The amount of ethanol in water affects the mixture density, viscosity and surface tension, as seen in Figure 11.

At lower water flow rates, the higher relative ethanol concentration causes the material properties of the ethanol to dominate. Ethanol mixes throughout the jet at lower water flow rates, causing an increase in viscosity and a decrease in surface tension. The increased viscosity enhances the transfer of the focusing gas shear force to the liquid, making the jet thinner and faster. At a water flow rate of 10 µl/min, the relative concentration of water and ethanol become similar. The viscosity and surface tension are similar to the lower water flow rate cases (Figure 11). This can be explained by the viscosity peak and a sharp decrease in surface tension, which occurs when the ethanol molar fraction is between 0.2 and 0.3 (Figure 2). Material properties of water become dominant at a further increase in water flow rate (20 µl/

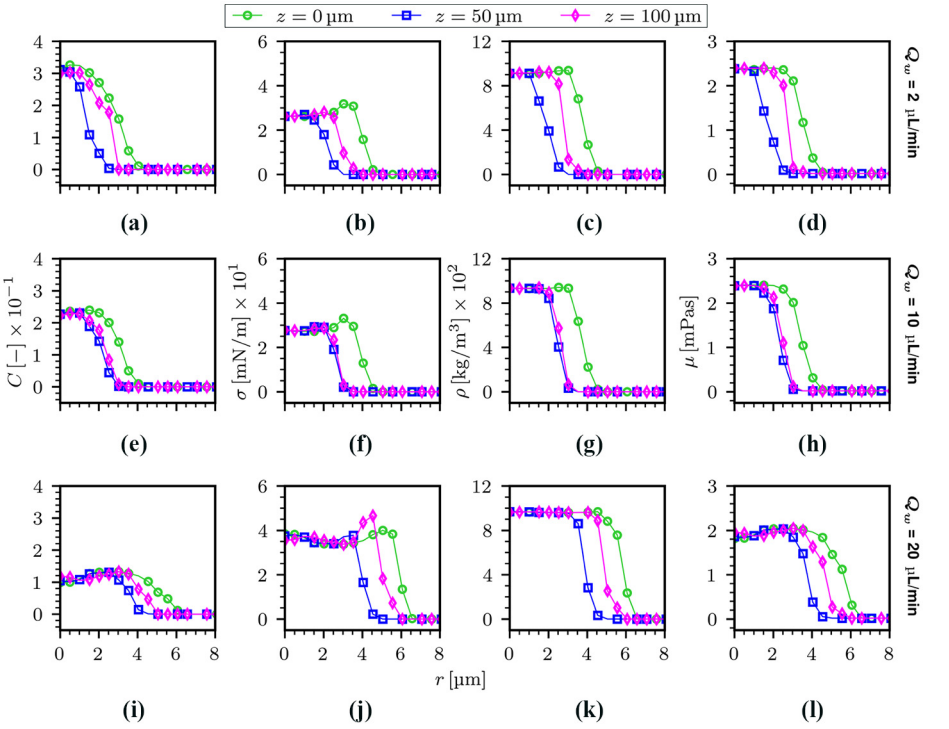

Notes: The ethanol and gas flow rates are kept constant at 10 µl/min and 5 mg/min, respectively. The water flow rate is changed as (a, b, c, d) 2 µl/min, (e, f, g, h) 10 µl/min and (i, j, k, l) 20 µl/min

Source: Figure by authors

Figure 11. Ethanol concentration, surface tension, density and viscosity in the radial direction at three axial positions of 0 µm, 50 µm and 100 µm downstream from the double flow focusing nozzle outlet

min), resulting in higher surface tension. The viscosity decreases, making the resulting jets thicker and slower (Zahoor *et al.*, 2024). The increase in jet length is attributed to the presence of a smaller viscosity of pure ethanol (Figure 11) in the outer layer of the jet. Such small viscosities make it easier for the surface instabilities to get convected downstream. The density of the mixture decreases almost linearly with the ethanol concentration.

Similarly to water, the changes in ethanol flow rates influence the relative concentration of ethanol in the mixture (Figure 12), impacting the resulting material properties of the mixture (Figure 13). It is seen that with the increase of ethanol flow rate, the material properties of ethanol start to become dominant. The required ethanol concentrations for viscosity peaks (molar fraction = approximately 0.2) are roughly reached at 8 µl/min of ethanol flow rate. The mixture moves towards ethanol saturation with a further increase, and the viscosity decreases. For ethanol flow rates of 16 µl/min and 20 µl/min, the liquid jets contain approximately 0.6–0.7 molar fraction of ethanol. This means that the viscosity reaches a maximum value of 2.4 mPas, while the surface tension is approximately 25 mNm^{-1}, lower than in pure water.

Figure 12 shows increased jet lengths and diameters for higher ethanol flow rates. The reason behind such an increase in jet lengths is that with higher ethanol flow rates, the mixture becomes ethanol-saturated, reaching inside the jet centre and resulting in viscosity peaks when mixed with water. A further increase in ethanol concentration (towards the outer surface) decreases the viscosity of the mixture. This helps the instability waves to get convected downstream and leads to longer jets.

No liquid jets are formed at a constant flow rate of 10 µl/min of water and ethanol if the gas flow rate is below 5 mg/min. High flow rates of both primary and secondary components

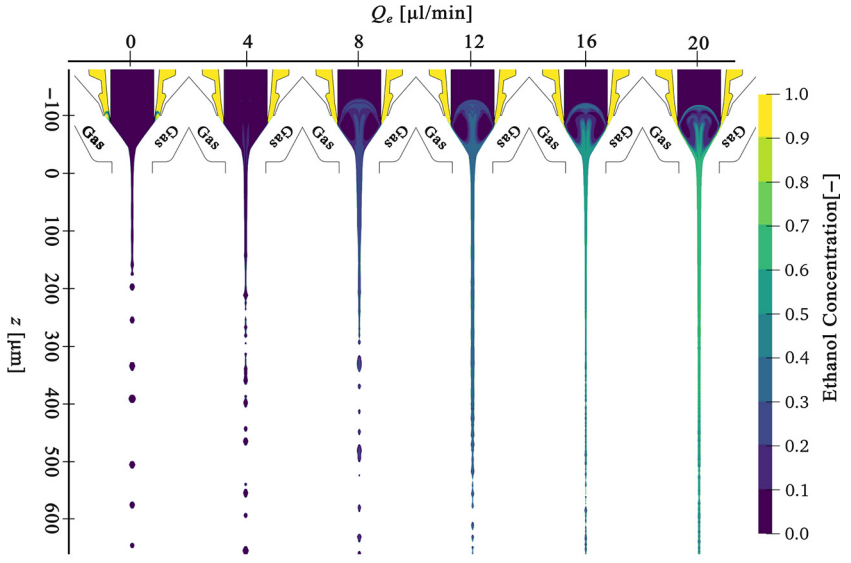

Source: Figure by authors

Figure 12. Comparison of micro-jet shape and ethanol concentration as a function of ethanol flow rate at constant water and gas flow rates of 10 µl/min and 5 mg/min, respectively

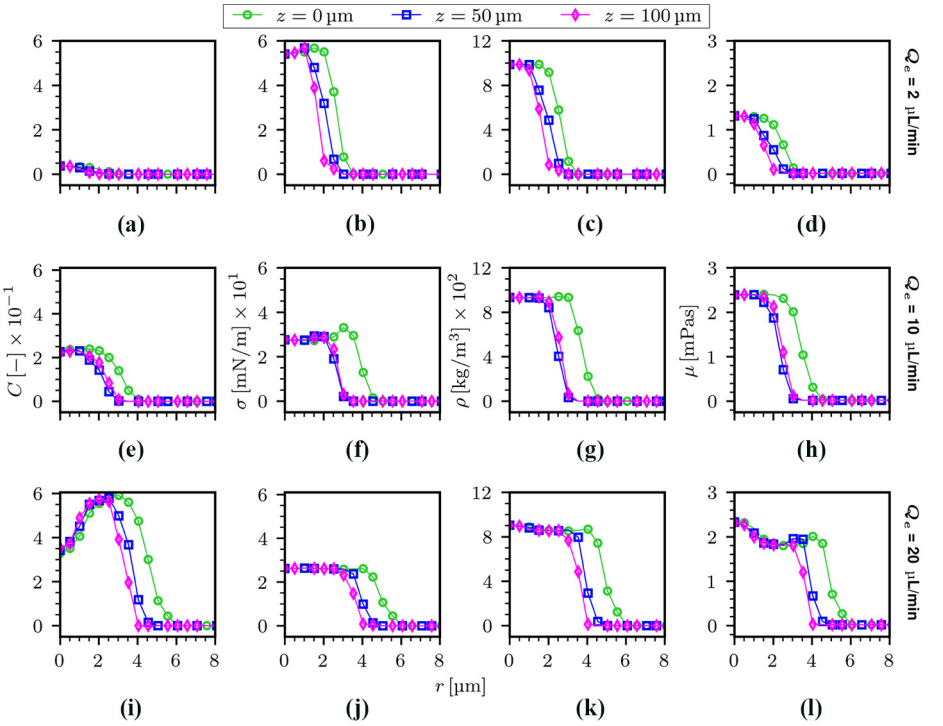

Notes: The water and gas flow rates are kept constant at 10 µl/min and 5 mg/min, respectively, while the ethanol flow rate is varied for (a, b, c, d) 2 µl/min, (e, f, g, h) 10 µl/min and (i, j, k, l) 20 µl/min

Source: Figure by authors

Figure 13. Ethanol concentration, surface tension, density and viscosity in the radial direction at three axial positions of 0 µm, 50 µm and 100 µm

require higher gas-focusing momentum. Figure 11 also shows that at liquid flow rates (10 µl/min), the viscosities are at a maximum throughout the jet, increasing the resistance to flow and requiring higher gas flow rates to produce and stabilise the jet.

Mixing of ethanol and water increases at a higher gas flow rate (Figure 14). The increased gas flow rate strengthens the liquid recirculation, causing more vigorous convective mixing.

4. Conclusions

An experimentally validated numerical study of DFFNs is presented. It is based on a mixture-continuum formulation, including coupled mass, momentum and species transport equations solved within the FVM-VOF framework. The considered liquid phase consists of water and ethanol with non-linear mixing. Based on the Jouyban–Acree model, the locally variable material properties were implemented to capture such convective-diffusive water–ethanol mixing. A comprehensive parametric study was conducted to independently assess the influence on mixing, material properties variations and the formation of jets as a function of flow parameters. Increasing

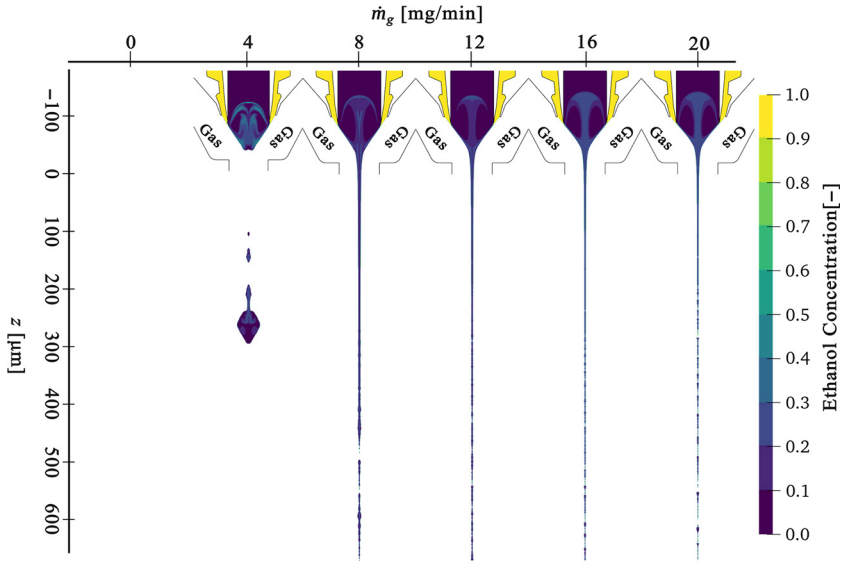

Source: Figure by authors

Figure 14. Comparison of micro-jet shape and ethanol concentration as a function of gas flow rate at constant water and ethanol flow rates of 10 µl/min and 10 µl/min, respectively

water and ethanol flow rates result in thicker, slower and longer jets. Increased gas flow rates result in thinner, faster and shorter jets. Our results demonstrate the importance of understanding and controlling mixture composition via water and ethanol flow rates, as this has a major effect on the stability and characteristics of the liquid jets. This study provides insight into DFFN operation, which is helpful in further development and optimisation of this type of sample delivery technique. Pre-mixed and linear mixing models substantially differ from the accurate representation of the water–ethanol mixing dynamics in DFFNs. Using the Jouyban–Acree mixing model highlights the importance of considering proper temporal and spatial non-linear mixing in double-flow-focused jets. The presented numerical study was conducted in incompressible and isothermal jet regimes. Further research will explore factors influencing jet characteristics, such as temperature, nozzle geometry and other fluids in primary and secondary capillaries. The compressible multiphase mixing model will additionally consider the energy equation with non-linear enthalpy of mixing, concentration and temperature-dependent specific heat, thermal conductivity, density, viscosity and surface tension, as well as the uncertainty analysis of the model.

References

Altarelli, M. (2011), "The European X-ray free-electron laser facility in Hamburg", *Nuclear Instruments and Methods in Physics Research Section B: Beam Interactions with Materials and Atoms*, Vol. 269 No. 24, pp. 2845-2849, doi: 10.1016/j.nimb.2011.04.034.

Barends, T.R.M., Stauch, B., Cherezov, V. and Schlichting, I. (2022), "Serial femtosecond crystallography", *Nature Reviews Methods Primers*, Vol. 2 No. 1, p. 59, doi: 10.1038/s43586-022-00141-7.

Baroud, C.N., Gallaire, F. and Dangla, R. (2010), "Dynamics of microfluidic droplets", *Lab on a Chip*, Vol. 10 No. 16, p. 2032, doi: 10.1039/c001191f.

Barty, A., Caleman, C., Aquila, A., Timneanu, N., Lomb, L., White, T.A., Andreasson, J., Arnlund, D., Bajt, S., Barends, T.R., Barthelmess, M., Bogan, M.J., Bostedt, C., Bozek, J.D., Coffee, R., Coppola, N., Davidsson, J., DePonte, D.P., Doak, R.B., Ekeberg, T., Elser, V., Epp, S.W., Erk, B., Fleckenstein, H., Foucar, L., Fromme, P., Graafsma, H., Gumprecht, L., Hajdu, J., Hampton, C. Y., Hartmann, R., Hartmann, A., Hauser, G., Hirsemann, H., Holl, P., Hunter, M.S., Johansson, L., Kassemeyer, S., Kimmel, N., Kirian, R.A., Liang, M., Maia, F.R.N.C., Malmerberg, E., Marchesini, S., Martin, A.V., Nass, K., Neutze, R., Reich, C., Rolles, D., Rudek, B., Rudenko, A., Scott, H., Schlichting, I., Schulz, J., Seibert, M.M., Shoeman, R.L., Sierra, R.G., Soltau, H., Spence, J.C.H., Stellato, F., Stern, S., Strüder, L., Ullrich, J., Wang, X., Weidenspointner, G., Weierstall, U., Wunderer, C.B. and Chapman, H.N. (2012), "Self-terminating diffraction gates femtosecond X-ray nanocrystallography measurements", *Nature Photonics*, Vol. 6 No. 1, pp. 35-40, doi: 10.1038/nphoton.2011.297.

Belšak, G., Bajt, S. and Šarler, B. (2021), "Numerical study of the micro-jet formation in double flow focusing nozzle geometry using different water-alcohol solutions", *Materials*, Vol. 14 No. 13, doi: 10.3390/ma14133614.

Botha, S. and Fromme, P. (2023), "Review of serial femtosecond crystallography including the COVID-19 pandemic impact and future outlook", *Structure*, Vol. 31 No. 11, pp. 1306-1319, doi: 10.1016/j.str.2023.10.005.

Brackbill, J.U., Kothe, D.B. and Zemach, C. (1992), "A continuum method for modeling surface tension", *Journal of Computational Physics*, Vol. 100 No. 2, pp. 335-354, doi: 10.1016/0021-9991(92)90240-Y.

Chapman, H.N., Fromme, P., Barty, A., White, T.A., Kirian, R.A., Aquila, A., Hunter, M.S., Schulz, J., DePonte, D.P., Weierstall, U., Doak, R.B., Maia, F.R.N.C., Martin, A.V., Schlichting, I., Lomb, L., Coppola, N., Shoeman, R.L., Epp, S.W., Hartmann, R., Rolles, D., Rudenko, A., Foucar, L., Kimmel, N., Weidenspointner, G., Holl, P., Liang, M., Barthelmess, M., Caleman, C., Boutet, S., Bogan, M.J., Krzywinski, J., Bostedt, C., Bajt, S., Gumprecht, L., Rudek, B., Erk, B., Schmidt, C., Hömke, A., Reich, C., Pietschner, D., Strüder, L., Hauser, G., Gorke, H., Ullrich, J., Herrmann, S., Schaller, G., Schopper, F., Soltau, H., Kühnel, K.U., Messerschmidt, M., Bozek, J. D., Hau-Riege, S.P., Frank, M., Hampton, C.Y., Sierra, R.G., Starodub, D., Williams, G.J., Hajdu, J., Timneanu, N., Seibert, M.M., Andreasson, J., Rocker, A., Jönsson, O., Svenda, M., Stern, S., Nass, K., Andritschke, R., Schröter, C.D., Krasniqi, F., Bott, M., Schmidt, K.E., Wang, X., Grotjohann, I., Holton, J.M., Barends, T.R.M., Neutze, R., Marchesini, S., Fromme, R., Schorb, S., Rupp, D., Adolph, M., Gorkhover, T., Andersson, I., Hirsemann, H., Potdevin, G., Graafsma, H., Nilsson, B. and Spence, J.C.H. (2011), "Femtosecond X-ray protein nanocrystallography", *Nature*, Vol. 470 No. 7332, pp. 73-77, doi: 10.1038/nature09750.

Courant, R., Friedrichs, K. and Lewy, H. (1967), "On the partial difference equations of mathematical physics", *IBM Journal of Research and Development*, Vol. 11 No. 2, pp. 215-234, doi: 10.1147/rd.112.0215.

DePonte, D.P., Weierstall, U., Schmidt, K., Warner, J., Starodub, D., Spence, J.C.H. and Doak, R.B. (2008), "Gas dynamic virtual nozzle for generation of microscopic droplet streams", *Journal of Physics D: Applied Physics*, Vol. 41 No. 19, p. 195505, doi: 10.1088/0022-3727/41/19/195505.

Ferziger, J.H. and Perić, M. (2002), *Computational Methods for Fluid Dynamics*, 3rd ed., Springer, Berlin.

Finehout, E. and Tian, W.C. (2009), *Microfluidics for Biological Applications*, Springer US, Boston, MA.

Fontana, F., Ferreira, M.P.A., Correia, A., Hirvonen, J. and Santos, H.A. (2016), "Microfluidics as a cutting-edge technique for drug delivery applications", *Journal of Drug Delivery Science and Technology*, Vol. 34, pp. 76-87, doi: 10.1016/j.jddst.2016.01.010.

Gañán-Calvo, A.M. (1998), "Generation of steady liquid microthreads and micron-sized monodisperse sprays in gas streams", *Physical Review Letters*, Vol. 80 No. 2, pp. 285-288, doi: 10.1103/PhysRevLett.80.285.

Gañán-Calvo, A.M., DePonte, D.P., Herrada, M.A., Spence, J.C.H., Weierstall, U. and Doak, R.B. (2010), "Liquid capillary micro/nanojets in free-jet expansion", *Small*, Vol. 6 No. 7, pp. 822-824, doi: 10.1002/smll.200901786.

Gañán-Calvo, A.M., González-Prieto, R., Riesco-Chueca, P., Herrada, M.A. and Flores-Mosquera, M. (2007), "Focusing capillary jets close to the continuum limit", *Nature Physics*, Vol. 3 No. 10, pp. 737-742, doi: 10.1038/nphys710.

Garstecki, P., Gitlin, I., Diluzio, W., Whitesides, G.M., Kumacheva, E. and Stone, H.A. (2004), "Formation of monodisperse bubbles in a microfluidic flow-focusing device", *Applied Physics Letters*, Vol. 85 No. 13, pp. 2649-2651, doi: 10.1063/1.1796526.

Greenshields, C.J. (2022), *OpenFOAM User Guide*, The OpenFOAM Foundation, London.

Günther, A. and Jensen, K.F. (2006), "Multiphase microfluidics: from flow characteristics to chemical and materials synthesis", *Lab on a Chip, Royal Society of Chemistry*, Vol. 6 No. 12, pp. 1487-1503.

Herrada, M.A., Gañán-Calvo, A.M., Ojeda-Monge, A., Bluth, B. and Riesco-Chueca, P. (2008), "Liquid flow focused by a gas: jetting, dripping, and recirculation", *Physical Review E*, Vol. 78 No. 3, p. 036323, doi: 10.1103/PhysRevE.78.036323.

Hirt, C.W. and Nichols, B.D. (1981), "Volume of fluid (VOF) method for the dynamics of free boundaries", *Journal of Computational Physics*, Vol. 39 No. 1, pp. 201-225, doi: 10.1016/0021-9991(81)90145-5.

Jouyban, A. and Acree, W.E. (1998), "Comparison of models for describing multiple peaks in solubility profiles", *International Journal of Pharmaceutics*, Vol. 167 No. 1-2, pp. 177-182, doi: 10.1016/S0378-5173(98)00073-8.

Jouyban, A. and Acree, W.E. (2021), "A single model to represent physico-chemical properties of liquid mixtures at various temperatures", *Journal of Molecular Liquids*, Vol. 323, p. 115054, doi: 10.1016/j.molliq.2020.115054.

Khattab, I.S., Bandarkar, F., Fakhree, M.A.A. and Jouyban, A. (2012), "Density, viscosity, and surface tension of water+ethanol mixtures from 293 to 323K", *Korean Journal of Chemical Engineering*, Vol. 29 No. 6, pp. 812-817, doi: 10.1007/s11814-011-0239-6.

Knoška, J., Adriano, L., Awel, S., Beyerlein, K.R., Yefanov, O., Oberthuer, D., Peña Murillo, G.E., Roth, N., Sarrou, I., Villanueva-Perez, P., Wiedorn, M.O., Wilde, F., Bajt, S., Chapman, H.N. and Heymann, M. (2020), "Ultracompact 3D microfluidics for time-resolved structural biology", *Nature Communications*, Vol. 11 No. 1, p. 657, doi: 10.1038/s41467-020-14434-6.

Koralek, J.D., Kim, J.B., Brůža, P., Curry, C.B., Chen, Z., Bechtel, H.A., Cordones, A.A., Sperling, P., Toleikis, S., Kern, J.F., Moeller, S.P., Glenzer, S.H. and DePonte, D.P. (2018), "Generation and characterization of ultrathin free-flowing liquid sheets", *Nature Communications*, Vol. 9 No. 1, p. 1353, doi: 10.1038/s41467-018-03696-w.

Kovačič, K., Gregorc, J. and Šarler, B. (2024), "Numerical modelling and experimental validation of dripping, jetting and whipping modes of gas dynamic virtual nozzle", *International Journal of Numerical Methods for Heat and Fluid Flow*, Vol. 34 No. 4, pp. 1582-1608, doi: 10.1108/HFF-09-2023-0573.

LeVeque, R.J. (2002), *Finite Volume Methods for Hyperbolic Problems*, Cambridge University Press, Cambridge.

Martiel, I., Müller-Werkmeister, H.M. and Cohen, A.E. (2019), "Strategies for sample delivery for femtosecond crystallography", *Acta Crystallographica Section D Structural Biology*, Vol. 75 No. 2, pp. 160-177, doi: 10.1107/S2059798318017953.

Montanero, J.M. (2024), *Tip Streaming of Simple and Complex Fluids*, Vol. 137 Springer Nature, Switzerland, Cham, doi: 10.1007/978-3-031-52768-5.

Moukalled, F., Mangani, L. and Darwish, M. (2016), *The Finite Volume Method in Computational Fluid Dynamics: An Advanced Introduction with OpenFOAM and Matlab*, Springer International Publishing.

Nelson, G., Kirian, R.A., Weierstall, U., Zatsepin, N.A., Faragó, T., Baumbach, T., Wilde, F., Niesler, F.B.P., Zimmer, B., Ishigami, I., Hikita, M., Bajt, S., Yeh, S.-R., Rousseau, D.L., Chapman, H.N., Spence, J.C.H. and Heymann, M. (2016), "Three-dimensional-printed gas dynamic virtual nozzles for x-ray laser sample delivery", *Optics Express*, Vol. 24 No. 11, p. 11515, doi: 10.1364/OE.24.011515.

Neutze, R., Wouts, R., van der Spoel, D., Weckert, E. and Hajdu, J. (2000), "Potential for biomolecular imaging with femtosecond X-ray pulses", *Nature*, Vol. 406 No. 6797, pp. 752-757, doi: 10.1038/35021099.

Nilghaz, A., Mousavi, S.M., Li, M., Tian, J., Cao, R. and Wang, X. (2021), "Paper based microfluidics for food safety and quality analysis", *Trends in Food Science and Technology*, Vol. 118, pp. 273-284.

Oberthuer, D., Knoška, J., Wiedorn, M.O., Beyerlein, K.R., Bushnell, D.A., Kovaleva, E.G., Heymann, M., Gumprecht, L., Kirian, R.A., Barty, A., Mariani, V., Tolstikova, A., Adriano, L., Awel, S., Barthelmess, M., Dörner, P., Xavier, L., Yefanov, O., James, D.R., Nelson, G., Wang, D., Calvey, G., Chen, Y., Schmidt, A., Szczepek, M., Frielingsdorf, S., Lenz, O., Snell, E., Robinson, P.J., Šarler, B., Belšak, G., Maček, M., Wilde, F., Aquila, A., Boutet, S., Liang, M., Hunter, M.S., Scheerer, P., Lipscomb, J.D., Weierstall, U., Kornberg, R.D., Spence, J.C.H., Pollack, L., Chapman, H.N. and Bajt, S. (2017), "Double-flow focused liquid injector for efficient serial femtosecond crystallography", *Scientific Reports*, Vol. 7 No. 1, p. 44628, doi: 10.1038/srep44628.

Rayleigh, L. (1879), "On the capillary phenomena of jets", *Proceedings of the Royal Society of London*, Vol. 29, pp. 71-97, doi: 10.1098/rspl.1879.0015.

Šarler, B., Zahoor, R. and Bajt, S. (2021), "Alternative geometric arrangements of the nozzle outlet orifice for liquid micro-jet focusing gas dynamic virtual nozzles", *Materials*, Vol. 14 No. 6, doi: 10.3390/ma14061572.

Schlichting, I. (2015), "Serial femtosecond crystallography: the first five years", *IUCrJ*, Vol. 2 No. 2, pp. 246-255, doi: 10.1107/S205225251402702X.

Sun, J., Warden, A.R. and Ding, X. (2019), "Recent advances in microfluidics for drug screening", *Biomicrofluidics*, Vol. 13 No. 6, p. 61503.

van Leer, B. (1979), "Towards the ultimate conservative difference scheme. V. A second-order sequel to Godunov's method", *Journal of Computational Physics*, Vol. 32 No. 1, pp. 101-136, doi: 10.1016/0021-9991(79)90145-1.

Vega, E.J., Montanero, J.M., Herrada, M.A. and Gañán-Calvo, A.M. (2010), "Global and local instability of flow focusing: the influence of the geometry", *Physics of Fluids*, Vol. 22 No. 6, pp. 1-10, doi: 10.1063/1.3450321.

Versteeg, H.K. and Malalasekera, W. (2007), *Fluid, An Introduction to Computational Dynamics: The Finite Volume Method*, 2nd ed., Pearson Education, Harlow.

Weierstall, U., Spence, J.C.H. and Doak, R.B. (2012), "Injector for scattering measurements on fully solvated biospecies", *Review of Scientific Instruments*, Vol. 83 No. 3, doi: 10.1063/1.3693040.

Weller, H.G. (2008), "A new approach to VOF-based interface capturing methods for incompressible and compressible Flow", Technical Report, No. May, p. 13.

Wiedorn, M.O., Oberthür, D., Bean, R., Schubert, R., Werner, N., Abbey, B., Aepfelbacher, M., Adriano, L., Allahgholi, A., Al-Qudami, N., Andreasson, J., Aplin, S., Awel, S., Ayyer, K., Bajt, S., Barák, I., Bari, S., Bielecki, J., Botha, S., Boukhelef, D., Brehm, W., Brockhauser, S., Cheviakov, I., Coleman, M.A., Cruz-Mazo, F., Danilevski, C., Darmanin, C., Doak, R.B., Domaracky, M., Dörner, K., Du, Y., Fangohr, H., Fleckenstein, H., Frank, M., Fromme, P., Gañán-Calvo, A.M., Gevorkov, Y., Giewekemeyer, K., Ginn, H.M., Graafsma, H., Graceffa, R., Greiffenberg, D., Gumprecht, L., Göttlicher, P., Hajdu, J., Hauf, S., Heymann, M., Holmes, S., Horke, D.A., Hunter, M.S., Imlau, S., Kaukher, A., Kim, Y., Klyuev, A., Knoška, J., Kobe, B., Kuhn, M., Kupitz, C., Küpper, J., Lahey-Rudolph, J.M., Laurus, T., Le Cong, K., Letrun, R., Xavier, P.L., Maia, L., Maia, F.R.N.C., Mariani, V., Messerschmidt, M., Metz, M., Mezza, D.,

Michelat, T., Mills, G., Monteiro, D.C.F., Morgan, A., Mühlig, K., Munke, A., Münnich, A., Nette, J., Nugent, K.A., Nuguid, T., Orville, A.M., Pandey, S., Pena, G., Villanueva-Perez, P., Poehlsen, J., Previtali, G., Redecke, L., Riekehr, W.M., Rohde, H., Round, A., Safenreiter, T., Sarrou, I., Sato, T., Schmidt, M., Schmitt, B., Schönherr, R., Schulz, J., Sellberg, J.A., Seibert, M. M., Seuring, C., Shelby, M.L., Shoeman, R.L., Sikorski, M., Silenzi, A., Stan, C.A., Shi, X., Stern, S., Sztuk-Dambietz, J., Szuba, J., Tolstikova, A., Trebbin, M., Trunk, U., Vagovic, P., Ve, T., Weinhausen, B., White, T.A., Wrona, K., Xu, C., Yefanov, O., Zatsepin, N., Zhang, J., Perbandt, M., Mancuso, A.P., Betzel, C., Chapman, H. and Barty, A. (2018), "Megahertz serial crystallography", *Nature Communications*, Vol. 9 No. 1, p. 4025, doi: 10.1038/s41467-018-06156-7.

Zahoor, R., Bajt, S. and Šarler, B. (2018a), "Influence of gas dynamic virtual nozzle geometry on micro-jet characteristics", *International Journal of Multiphase Flow*, Vol. 104, pp. 152-165, doi: 10.1016/j.ijmultiphaseflow.2018.03.003.

Zahoor, R., Bajt, S. and Šarler, B. (2018b), "Numerical investigation on influence of focusing gas type on liquid micro-jet characteristics", *International Journal of Hydromechatronics*, Vol. 1 No. 2, p. 222, doi: 10.1504/IJHM.2018.092732.

Zahoor, R., Belšak, G., Bajt, S. and Šarler, B. (2018c), "Simulation of liquid micro-jet in free expanding high speed co-flowing gas streams", *Microfluidics and Nanofluidics*, Vol. 22 No. 8, p. 87, doi: 10.1007/s10404-018-2110-0.

Zahoor, R., Regvar, R., Bajt, S. and Šarler, B. (2020), "A numerical study on the influence of liquid properties on gas-focused micro-jets", *Progress in Computational Fluid Dynamics, An International Journal*, Vol. 20 No. 2, pp. 71-83, doi: 10.1504/PCFD.2020.106407.

Zahoor, R., Knoška, J., Bajt, S. and Šarler, B. (2021), "Experimental and numerical investigation of gas-focused liquid micro-jet velocity", *International Journal of Multiphase Flow*, Vol. 135, p. 103530, doi: 10.1016/j.ijmultiphaseflow.2020.103530.

Zahoor, R., Bajt, S. and Šarler, B. (2024), "A numerical study of gas focused non-Newtonian micro-jets", *International Journal of Multiphase Flow*, Vol. 170, p. 104628, doi: 10.1016/j.ijmultiphaseflow.2023.104628.

Corresponding author
Božidar Šarler can be contacted at: bozidar.sarler@fs.uni-lj.si